JACS
JOURNAL OF THE AMERICAN CHEMICAL SOCIETY
pubs.acs.org/JACS
Article

Coupling of the Structure and Magnetism to Spin Splitting in Hybrid Organic−Inorganic Perovskites

Ravi Kashikar,* Derick DeTellem, Partha Sarathi Ghosh, Yixuan Xu, Shengqian Ma, Sarath Witanachchi, Manh-Huong Phan, Sergey Lisenkov, and Inna Ponomareva*

Cite This: J. Am. Chem. Soc. 2024, 146, 13105−13112
Read Online

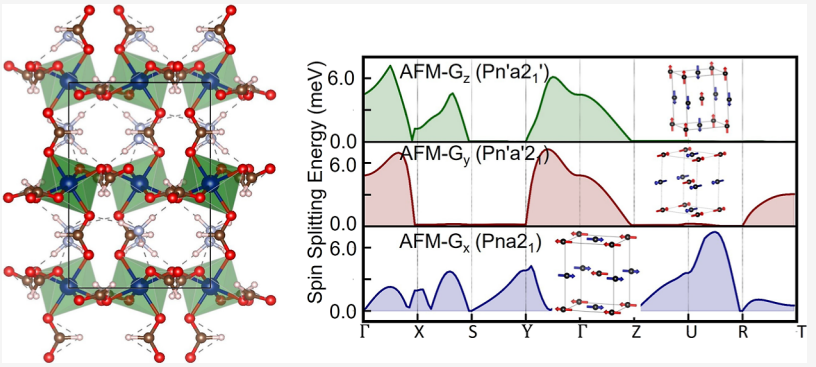

ABSTRACT: Hybrid organic−inorganic perovskites are famous for the diversity of their chemical compositions, phases, phase transitions, and associated physical properties. We use a combination of experimental and computational techniques to reveal a strong coupling between structure, magnetism, and spin splitting in a representative of the largest family of hybrid organic−inorganic perovskites: the formates. With the help of first-principles simulations, we find spin splitting in both conduction and valence bands of $[NH_2NH_3]Co(HCOO)_3$ induced by spin−orbit interactions, which can reach up to 14 meV. Our magnetic measurements reveal that this material exhibits canted antiferromagnetism below 15.5 K. The direction of the associated antiferromagnetic order parameter is strongly coupled with spin splitting in the centrosymmetric phase, allowing for the creation and annihilation of spin splitting through the application of a magnetic field. Furthermore, the structural phase transition to the experimentally observed polar $Pna2_1$ phase completely changes the aforementioned spin splitting and its coupling to magnetic degrees of freedom. This reveals that in $[NH_2NH_3]Co(HCOO)_3$, the structure and magnetism are strongly coupled to spin splitting and can be manipulated through electric and magnetic fields. We believe that our findings offer an important step toward a fundamental understanding and practical applications of materials with coupled properties.

INTRODUCTION

The ability to couple structural and magnetic degrees of freedom to materials properties is of tremendous scientific and technological importance. For example, coupling between structural and electron spin degrees of freedom is promising for applications in spintronics.[1,2] One of the ways to access spin degrees of freedom is through spin−orbit interaction, which breaks the Hamiltonian symmetry and splits spin-degenerate bands.[3,4] Spin−orbit interactions in solids give origin to the so-called Rashba and Dresselhaus effects, which originate from structural inversion asymmetry and bulk inversion asymmetry, respectively.[3,5−7] These effects give origin to spin splitting in the electronic bands and, consequently, the opportunity to access a particular spin channel and also lead to the emergence of spin texturing in either real or reciprocal space. Certain types of spin textures are known to enhance spin states' lifetimes and, therefore, are critical for applications in spintronics.[8−10] Structural degrees of freedom are typically associated with ionic positions and lattice vectors and can be manipulated through temperature and external fields.[11] Ferroics usually offer great opportunities for structural manipulations, as they have a tendency to undergo phase transitions and often couple to electric fields. Magnetic degrees of freedom are usually associated with localized spins and may be either disordered or ordered. Examples are paramagnetism and (anti) ferromagnetism, respectively. While ferromagnetism results in spin-dependent electronic band

Received: December 27, 2023
Revised: April 15, 2024
Accepted: April 16, 2024
Published: May 1, 2024

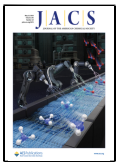

https://doi.org/10.1021/jacs.3c14744
J. Am. Chem. Soc. 2024, 146, 13105−13112

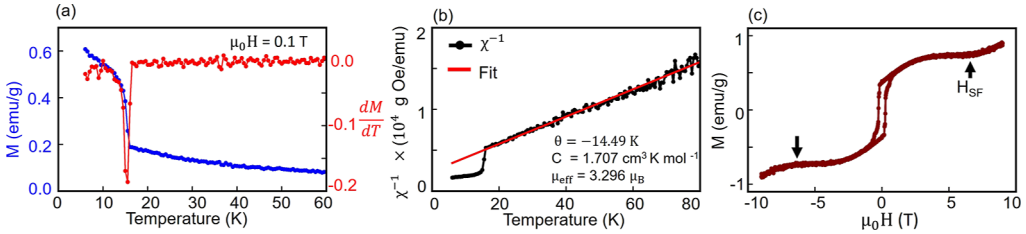

Figure 1. (a) Temperature dependence of the magnetization (blue) and its derivative dM/dT (red); (b) inverse susceptibility as a function of temperature $\chi^{-1}(T)$ and a fit to the Curie−Weiss law (red line); and (c) magnetic field dependence of the magnetization curve taken at 10 K, showing a ferromagnetic hysteresis at low fields and a spin-flop transition around 6.5 T.

structures, more subtle effect of spin splitting has been predicted from group theoretical analysis in antiferromagnetic (AFM) materials.[12−19] Remarkably, some AFM materials can exhibit spin splitting even in the absence of spin−orbit interactions.[12] Recently, a novel class of magnetic materials known as altermagnets has emerged. These materials are collinear antiferromagnets, where spin sublattices are connected by proper or improper spatial rotation operations and exhibit spin splitting in their electronic bands in the momentum space, in the absence of spin−orbit coupling (SOC).[20−22] It appears that materials in the ferroic, or more precisely multiferroic, family may have significant potential for coupling structure and magnetic ordering to spin splitting. This motivated us to look into the hybrid organic−inorganic perovskite class of materials, that share the chemical formula ABX_3, where A typically is an organic cation and B is an inorganic cation, while X could be either organic or inorganic.[23] In particular, we will look into one of the largest families in this class: hybrid formate perovskites with chemical formula $AB(HCOO)_3$.[24] What makes them attractive for our search of materials with coupled degrees of freedom is that many of them exhibit AFM ordering and many undergo phase transitions into polar space groups above room temperature.[25] For example, $[NH_2NH_3][Co(HCOO)_3]$ and $[CH_3NH_2NH_2][Mn(HCOO)_3]$ exhibit transitions into polar phases below 363 and 309 K, respectively.[26,27] Ferroelectricity in $[NH_2NH_3][Co(HCOO)_3]$ was reported in ref 28, while ferroelectric ordering in $[CH_3NH_2NH_2][Mn(HCOO)_3]$ was suggested from pyroelectric measurements.[27] Furthermore, we can find multiferroics with desired features of AFM in $[(CH_3)_2NH_2]M(HCOO)_3$ (M = Mn, Fe, Co, Ni) and $NH_4M(HCOO)_3$ (M = Mn, Co) family.[25] Among them, one promising candidate for coupling between multiple degrees of freedom to spin splitting is $[NH_2NH_3]Co(HCOO)_3$. It exhibits a high-temperature *Pnma* phase and undergoes a phase transition to the polar $Pna2_1$ phase at 363 K.[29] As a result, it is predicted to be ferroelectric at room temperature with a remnant polarization of 2.6 $\mu C/cm^2$.[28] The structural phase transition in this compound is driven by the hydrogen bond stabilization.[28] $[NH_2NH_3]Co(HCOO)_3$ also exhibits competing, possibly antipolar, $P2_12_12_1$ phases, which show spin-canted AFM long-range ordering, with Néel temperatures of 13.9 K.[26] Therefore, it may exhibit the desired coupling of structure and magnetism to spin splitting.

Previously, spin splitting coupled to the direction of polarization and AFM order parameters, tunable by both magnetic ordering and polarization direction, has been predicted in hybrid organic−inorganic perovskite TMCM-$MnCl_3$.[30] Recently, Yananose et al. have examined $C(NH_2)_3]$-$M(HCOO)_3$ (M = Cr, Cu) and predicted the persistent and irregular spin texture.[31] Among nonmagnetic hybrid perovskites, TMCM-$CdCl_3$ and $MPSnBr_3$ exhibit persistent spin texture in the valence band and conduction band, respectively.[32,33] However, what is presently missing is an understanding of the interplay between structural and magnetic degrees of freedom in the establishment of spin splitting in hybrid organic−inorganic perovskites.

The goal of this study is to utilize a combination of computational and experimental tools to (i) predict the existence of spin splitting in hybrid formate perovskites, which is strongly coupled to both structural and magnetic degrees of freedom; (ii) reveal the possibility to create, annihilate, and manipulate spin splitting through application of electric and magnetic fields; (iii) rationalize our findings through decoupling contributions from different degrees of freedom; and (iv) propose practical ways to achieve spin-splitting manipulation in such materials.

EXPERIMENTAL AND COMPUTATIONAL DETAILS

$[NH_2NH_3]Co(HCOO)_3$ was synthesized by using the mild solution method. The solvent diffusion was carried out using $Co(No_3)2.6H_2O$ (1.0 mmol, 0.291 g) in 5.0 mL of methanol solution. Later, it was layered onto 5.0 mL methanol with 95% (78 mmol, 3.2 mL) formic acid and 98% (6.2 mmol, 0.6 mL) hydrazine monohydrate. The magenta-colored rectangular crystals were obtained after 24 h, which were separated from the bulk phase and washed with reagent-grade ethanol after the mother solvent was removed. The perovskite structures were confirmed with single-crystal X-ray diffraction measurements. Magnetic measurements were carried out in a Quantum Design DynaCool Physical Property Measurement System (PPMS) using a vibrating sample magnetometer with the magnetic field aligned parallel to the $a-b$ plane. Magnetization vs applied field, $M(H)$, was measured at 10 K, with an applied field of 9 T. Magnetization vs temperature, $M(T)$, was measured between 5 and 100 K, using the zero-field-cooled warming protocol and under 0.1 T applied field.

For computations, we used spin-polarized density functional theory (DFT) as implemented in the Vienna Ab initio Simulation Package with a Perdew−Burke−Ernzerhof exchange−correlation functional.[34−36] The energy cutoff was set to 700 eV for the plane-wave basis, and the Brillouin zone integration was carried out using a gamma-centered k-mesh of 5 × 5 × 3. We used U_{eff} = 2.0 eV correction for Co-d states as proposed by Dudarev et al.[37] The zero-damping DFT-D3 approach, proposed by Grimme et al., was employed to incorporate the van der Waals interactions.[38] Structural relaxations were performed using a conjugate gradient algorithm until the forces on each atom were less than 1 meV/Å while stresses were less than 0.001 GPa. The electronic structure calculations were performed with SOC both on and off. The electric polarization was computed using the modern theory of polarization developed by King-Smith and Vanderbilt.[39]

https://doi.org/10.1021/jacs.3c14744
J. Am. Chem. Soc. 2024, 146, 13105−13112

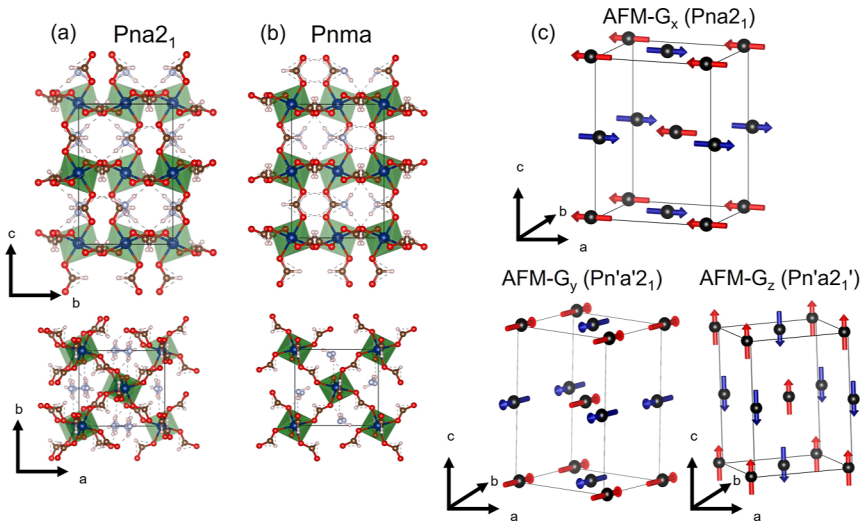

Figure 2. Crystal structure of $[NH_2NH_3]Co(HCOO)_3$ in *Pna*2$_1$ and *Pnma* phases in different cross sections (a,b). Magnetic moment arrangements in G-AFM ordering and corresponding magnetic space group (c).

RESULTS AND DISCUSSION

Although AFM ordering has been reported for $[NH_2NH_3]Co(HCOO)_3$ in the $P2_12_12_1$ phase,[26] no reports are available for the polar *Pna*2$_1$ phase. Our magnetic data analysis for the *Pna*2$_1$ phase is given in Figure 1, which suggests canted AFM ordering below 15.5 K. Figure 1a shows the temperature dependence of magnetization along with its derivative, dM/dT, revealing a magnetic-phase transition at 15.5 K. Inverse susceptibility χ^{-1} was calculated from this data $H/M(T)$ and fit with the Curie−Weiss law, $\chi = C/(T - \theta)$ (Figure 1b), where a Curie−Weiss temperature of $\theta = -14.49$ K was obtained. It is clear that at high temperatures in the paramagnetic regime, the $\chi^{-1}(T)$ data obeys the Curie−Weiss law. The negative value of θ confirms AFM couplings between adjacent Co^{2+} ions and that the phase transition at $T_N \sim 15.5$ K is AFM in nature. We note that formates typically have low magnetic transition temperatures, as it is believed that formate linkers can only mediate weak magnetic interactions.[23] From the Curie constant obtained through the fit ($C = 1.707$ cm^3 K mol^{-1}), an effective magnetic moment of $\mu_{eff} \sim 3.296$ μ_B/Co is obtained, using the relation $C = N_A\mu_B^2\mu_{eff}^2/3k_B$. It is also worth noting from Figure 1b that there is a sudden decline in χ^{-1} at ∼15 K, signaling the characteristic of a spin-canted AFM system.[40−42] To confirm the occurrence of spin canting in $[NH_2NH_3]Co(HCOO)_3$, the magnetic field dependence of magnetization $M(H)$ was measured at temperatures below the T_N. Figure 1c displays such a $M(H)$ loop taken at 10 K, confirming that there is a small canted AFM moment at low fields of ∼0.4 emu/g, with a coercive field of 0.25 T. When the applied magnetic field exceeds $H_{SF} \sim 6.5$ T, there is an increase in the magnetization characteristic of a spin-flop transition (Figure 1c).[40] This provides further evidence for the spin-canted AFM order in $[NH_2NH_3]Co(HCOO)_3$.[26] The spin-canted AFM behavior was also observed in $Cu_3(TeO_4)(SO_4)\cdot H_2O$[40] and $\{Co(N_3)(bpmb)(H_2O)_2\cdot H_2O\}_n$.[41] Thus, low-temperature $[NH_2NH_3]Co(HCOO)_3$ in the *Pna*2$_1$ phase is multiferroic as it exhibits the coexistence of electric (spontaneous polarization) and magnetic orderings. As a result, it could potentially exhibit spin splitting due to AFM ordering and noncentrosymmetric nature.

To determine whether these two orderings are indeed capable of inducing spin splitting in this material, we turn to simulations. To decouple the contributions from magnetic and electric orderings, both centrosymmetric and noncentrosymmetric structures are required. To obtain the noncentrosymmetric phase, we carried out the structural relaxation of the *Pna*2$_1$ phase reported in ref 28. The structure is visualized in Figure 2a. The ground state was shown to be G-type AFM in ref 28. Therefore, we use G-type AFM arrangements of magnetic moments on Co atoms but simulate three different orientations of the magnetic moments: along the *x*, *y*, and *z* directions, as shown in Figure 2c. Note that the axes of our Cartesian coordinate system are aligned along the crystallographic *a*, *b*, and *c* axis. It should be noted that we do not find canted magnetic moment in computations, which could be due to both our computational resolution and the size of the supercell. The centrosymmetric structure for $[NH_2NH_3]Co(HCOO)_3$ is *Pnma*, which is also a high-temperature phase reported in ref 28. However, it is a disordered phase with partial occupancies and, therefore, cannot be used in simulations. To construct a prototype of such a phase that does not have partial occupancy but still has experimental relevance, we create a polarization reversal path for the *Pna*2$_1$ phase following ref 43. The structure that corresponds to zero polarization is the centrosymmetric *Pnma* phase. This structure is next subjected to full structural relaxation, which preserves the space group. The structure is visualized in Figure 2b. Experimentally, such a phase could occur during polarization reversal at fields close to the coercive field. At zero Kelvin, the *Pnma* structure is 280 meV/f.u. higher in energy than the ground state. The structural relaxation has been carried out for different types of magnetic orderings: ferromagnetic, A-type, C-type, and G-type AFM orderings, and it was found that the G-type AFM ordering is the lowest in energy. Furthermore, we considered G-type AFM orderings with different directions of magnetic moments, resulting in the alignment of the AFM vector along *x*, *y*, or *z* directions, as shown in Figure 2c. We found that AFM-G$_x$ (*Pnma*) has the lowest energy followed by AFM-G$_z$ (*Pn*′*ma*′) and AFM-G$_y$ (*Pn*′*m*′*a*), with 0.002 and 0.02 meV/f.u. higher energy, respectively. The structures are provided in ref 44.

https://doi.org/10.1021/jacs.3c14744
J. Am. Chem. Soc. 2024, 146, 13105−13112

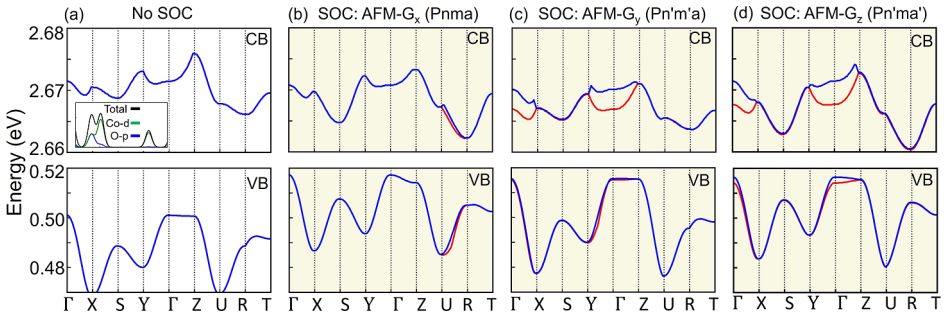

Figure 3. Band structure of $[NH_2NH_3]Co(HCOO)_3$ in the *Pnma* phase without (a) and with (b–d) SOC.

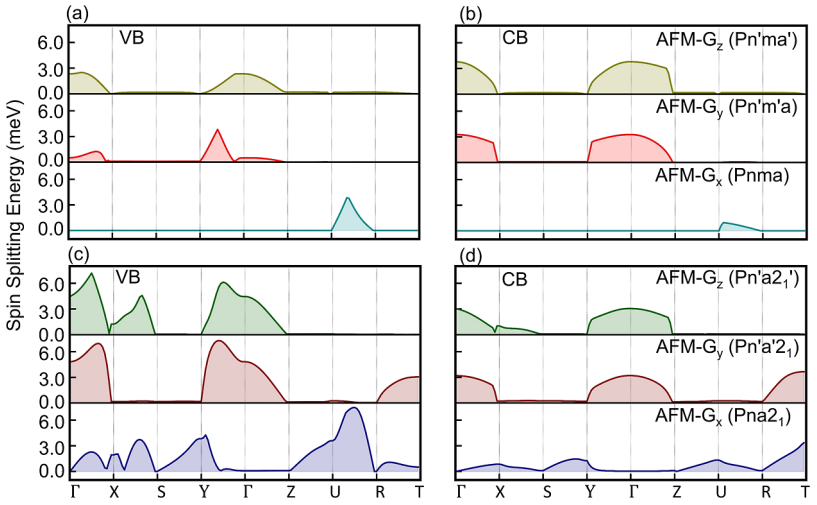

Figure 4. Spin splitting between the top two VBs (a,c) and bottom two CBs (b,d) along the high-symmetry *k*-path in different phases of $[NH_2NH_3]Co(HCOO)_3$.

The magnetic space groups *Pn′m′a*, *Pn′ma′*, and *Pnma* do not possess ΘI symmetry and, therefore, may exhibit SOC-induced spin splitting.[12] Here, Θ and I are time-reversal and spatial inversion symmetries. Moreover, these magnetic space groups belong to types III, III, and I, respectively, which allow for AFM-induced spin splitting, as proposed in ref 12. Following the classification of ref 15, they belong to spin split type-4A and allow for spin splitting with or without SOC, based on the symmetry considerations. To explore that, we carried out DFT computations of electronic structure with SOC turned off and on. Of course, when SOC is turned off, we use spin-polarized computations. Figure 3 presents our data for both cases. We find no spin splitting in the absence of an SOC along the chosen directions. The partial density of states shown in the inset of Figure 3a infers that bands near the Fermi level are from Co-d states. In addition, the O-p states are populated at the valence-band region. Among the Co-d states, d_{xy} and d_{z^2} have double occupancy, and hence, they peak in the valence-band spectrum. The remaining d orbitals have a single occupancy, thus offering a magnetic moment of 2.68 μ_B at each Co site.

Turning SOC on results in spin splitting (Figure 3b–d), which shows a strong dependence on the direction of the AFM order parameter. To quantify such dependence, we compute spin splitting along the different directions of the Brillouin zone and present it in Figure 4.

Figure 4 confirms spin-splitting dependence on the direction of the AFM order parameter throughout the Brillouin zone. For example, the spin splitting along *Y*-Γ-*Z* direction in CB can be turned on or off by switching the AFM vector between the y or the z direction. Similar trends are observed in VB. Experimentally, the change of the AFM vector direction can be achieved through the spin-flop mechanism, which opens the possibility to create/erase or tune spin splitting by the application of a magnetic field. For instance, the field at which the spin-flop transition occurs is 6.5 T for a T of 10 K (Figure 1c). We note that the magnitude of spin splitting also shows a strong dependence on the direction of the AFM vector. Thus, our simulations on the centrosymmetric-phase prototype for AFM $[NH_2NH_3]Co(HCOO)_3$ revealed (i) the presence of SOC-induced spin splitting up to 4 meV in both CB and VB and (ii) strong dependence of spin-splitting magnitude on the direction of the AFM vector, which allows for both creation and erasing of spin splitting, as well as its manipulations by the magnetic field. Next, we turn to an investigation of the role that spatial asymmetry plays in spin splitting and the aforementioned findings. Removal of the mirror plane perpendicular to the *c*-axis results in the ground-state structure of $[NH_2NH_3]Co(HCOO)_3$ with the $Pna2_1$ space group. Introducing G-type AFM ordering with different directions of the **G** vector followed by full structural relaxation resulted in the structures with magnetic space groups $Pna2_1$, $Pn'a'2_1$, and $Pn'a2_1'$ for AFM-G_x, AFM-G_y, and AFM-G_z, respectively. Energetically, AFM-G_x has the lowest energy, followed by AFM-G_z (0.18 meV/f.u.) and AFM-G_y (0.47 meV/f.u.). All these structures belong to the spin splitting type-4B as per classification of ref 15, and by symmetry, allow

https://doi.org/10.1021/jacs.3c14744
J. Am. Chem. Soc. 2024, 146, 13105−13112

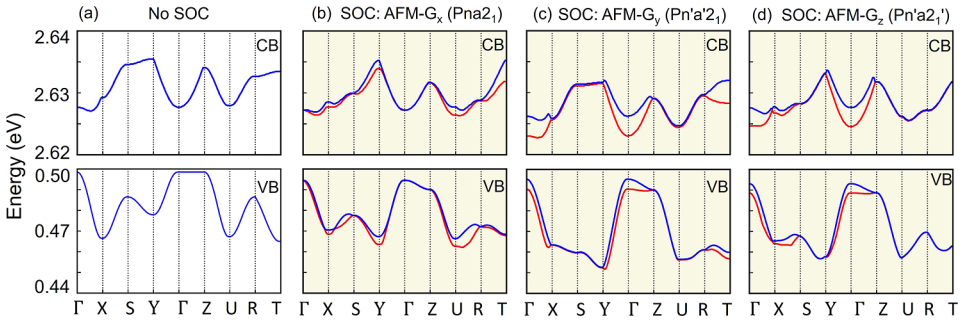

Figure 5. Band structure of *Pna*2$_1$ $[NH_2NH_3]Co(HCOO)_3$ without SOC (a) and with SOC in (b–d) for *x*, *y*, and *z* spin orientations of AFM-G magnetic ordering.

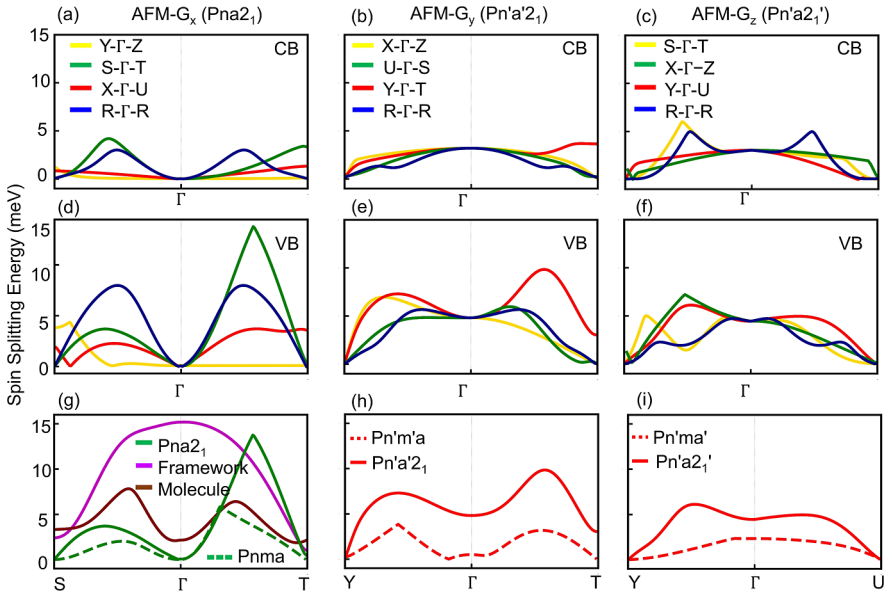

Figure 6. Spin splitting along various *k*-paths in the Brillouin zone of the polar phases of $[NH_2NH_3]Co(HCOO)_3$ for the lowermost conduction bands (a–c) and uppermost valence bands (d–f) for *x*, *y*, and *z* orientations for the AFM order parameter. Comparison of the uppermost VB spin splitting for centrosymmetric and polar phases (g–i).

for spin splitting with and without SOC. Figure 5 presents the electronic structure calculations for both of these cases.

Again, we find that AFM on its own is not capable of inducing spin splitting in this material along the chosen directions in the Brillouin zone. However, the introduction of SOC results in such spin splitting for all directions of the AFM vector considered here. Moreover, just like before, we find that both magnitudes of spin splitting in its location in the Brillouin zone exhibit strong dependence on the direction of the AFM vector. This is quantified in Figure 4. The magnitude of spin splitting is up to 7 meV in CB and up to 4 meV in VB, which offers enhancement with respect to centrosymmetric phases. We find a direct band gap of 2.1 eV, which is likely to underestimate the true band gap, as known for DFT. Remarkably, the bands are spin-split at VBM and CBM (located at the Γ point) despite being in the time-reversal invariant momenta point. This is the consequence of the AFM ordering, discussed in refs 12 and 15. It is also a rare but technologically significant property. Comparison between our data for centrosymmetric and noncentrosymmetric phases with different magnetic order parameter directions (see Figure 4) reveals that $[NH_2NH_3]Co(HCOO)_3$ exhibits strong coupling between multiple degrees of freedom: structural, magnetic, and spin splitting. For example, in the Γ point of VB, spin splitting is zero for AFM-G$_x$. It can be turned on by aligning the AFM vector along the *y*-axis, via a spin-flop mechanism induced by a magnetic field. Inducing the centrosymmetric phase through an electric field (during polarization reversal, for example) or temperature manipulations will result in near disappearance of spin splitting. Likewise, the noncentrosymmetric polar phase can be induced by the application of an electric field, which will change spin splitting from the ones shown in Figure 4a,b to the ones shown in Figure 4c,d. Figure 4 also reveals greater overlap in the spin-splitting peaks between space groups containing time-reversed symmetry elements as compared to those that do not, suggesting strong contributions to spin splitting from AFM.

To find out whether even larger values of spin splitting can be achieved in the vicinity of the VBM and CBM as well as to assess anisotropy of the spin splitting, we explore several directions in the vicinity of the CBM and VBM. Figure 6 gives spin splitting along the directions investigated. The largest value can reach 14 meV in VB and occurs between Γ and *T*. It is comparable with the 27 meV reported for the TMCM-$MnCl_3$ hybrid perovskite.[30] To estimate the contribution to spin splitting from antiferromagnetism, we overlap the data for centrosymmetric and noncentrosymmetric structures in Figure 6g–i. For this analysis, the path in the Brillouin zone

https://doi.org/10.1021/jacs.3c14744
J. Am. Chem. Soc. 2024, 146, 13105–13112

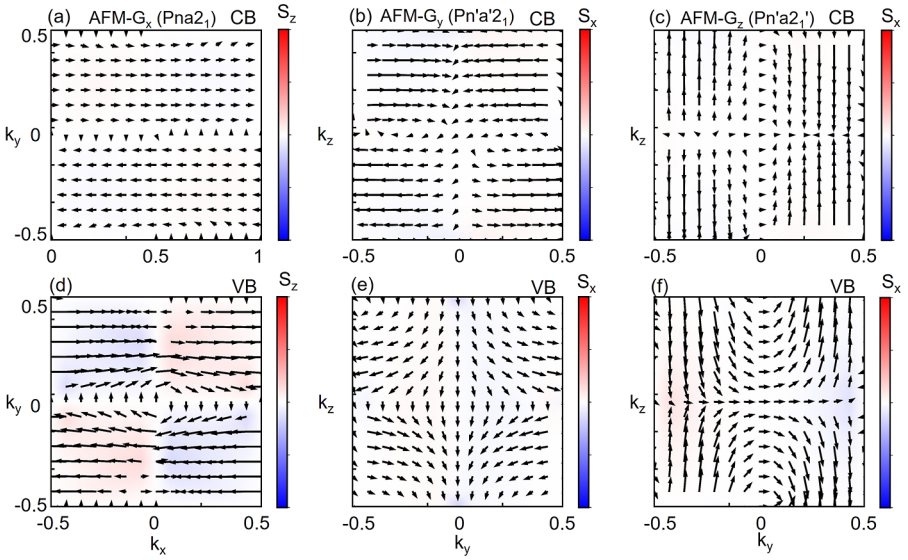

Figure 7. Spin textures around the CBM (a–c) and VBM (d–f) in various *k*-planes for the polar phases of $[NH_2NH_3]Co(HCOO)_3$.

associated with the largest spin splitting is chosen. From this comparison, we conclude that AFM makes a significant contribution to spin splitting in all cases. Further analysis can be carried out to decouple structural contribution to spin splitting into contributions from the $[NH_2NH_3]^{-1}$ molecule and the $Co(HCOO)_3$ framework. To compute the contribution due to the molecule, we keep the framework in its *Pnma* structure, while molecules are in their *Pna*2$_1$ configuration. To compute contributions due to the framework, we keep molecules in their *Pnma* positions while the framework is in the *Pna*2$_1$ structure.[45−47] The decomposition is shown in Figure 6g. We can see that the largest contribution to the spin splitting comes from the framework. For a tentative explanation of such a finding, we decompose the polarization of the *Pna*2$_1$ phase into contributions from the molecule and the framework. The framework contributes 73% to the total polarization, while the molecule contributes 27%. Therefore, it may be that structural distortions of the framework make the largest contribution to the local electric field and are responsible for the spin−orbit interaction and associated spin splitting.

Figure 7 shows spin textures in the CB and VB for *Pna*2$_1$-type structures. We find that the type of spin texture is fully coupled to the direction of the AFM vector. Interestingly, for the *Pna*2$_1$ structure with AFM-G$_x$ orientation, the spin textures are mostly persistent in a large portion of the Brillouin zone, which is highly desirable for the application of spintronics. Switching the direction of the AFM order parameter changes the type of spin textures and, therefore, will cause relaxation.

In order to find out whether the discussed findings are specific to $[NH_2NH_3]Co(HCOO)_3$ or likely to occur in other materials from the same family, we have repeated calculations for $[NH_2NH_3]Mn(HCOO)_3$. This material exhibits a canted AFM phase below 7.9 K and undergoes a polar (*Pna*2$_1$) to nonpolar (*Pnma*) phase transition at 355 K,[26] similar to the case of $[NH_2NH_3]Co(HCOO)_3$. All computational approaches remained the same except that we used U_{eff} = 4.0 eV for Mn. The structures are provided in ref 44. The simulated electronic structure for *Pnma* and *Pna*2$_1$ phases are shown in Figures S1 and S2 of the Supporting Information for *x*, *y*, and *z* orientation of the AFM order parameter. In both cases, we observed spin splitting in the conduction and valence bands. The magnitude of the spin splitting is 4 meV, near Γ for VB for both phases. The magnitude of the spin splitting varies with the magnetic moment directions. The dependence of spin splitting in VB and CB on the direction of the AFM vector of both phases is shown in Figure S3. The spin texture around the VBM for $[NH_2NH_3]Mn(HCOO)_3$ is persistent in nature (see Figure S4 of the Supporting Information). Thus, $[NH_2NH_3]Mn(HCOO)_3$ also exhibits the main features established for $[NH_2NH_3]Co(HCOO)_3$. These include strong coupling between structural, magnetic, and spin degrees of freedom; the presence of spin splitting even in the centrosymmetric phase of the material; and persistent spin textures.

SUMMARY

In summary, we have synthesized $[NH_2NH_3]Co(HCOO)_3$ in the polar *Pna*2$_1$ space group and found it to be a canted antiferromagnet below 15.5 K. DFT computations were then utilized to predict spin splitting in this compound. Interestingly, SOC-induced spin splitting exists already in the prototype of the centrosymmetric phase of the material and even in the time-reversal invariant momenta points of the Brillouin zone. These findings originate from AFM ordering. The spin splitting couples strongly to the direction of the AFM vector and can be turned on or off through AFM vector reorientation, which opens a way to spin-splitting tunability by the application of a magnetic field, for example, via a spin-flop mechanism. Phase transition from the centrosymmetric to the polar phase of the material results in a dramatic change in the spin-splitting landscape in the Brillouin zone, thus offering additional tunability by the electric field or temperature. For example, a macroscopically centrosymmetric phase can be achieved at low temperatures during an electric-field-induced polarization reversal. Just as in the prototypical centrosymmetric phase of the material, the polar phase exhibits a strong dependence of the spin splitting on the direction of the AFM vector. Thus, our work reveals that the low-temperature polar phase of $[NH_2NH_3]Co(HCOO)_3$ (and $[NH_2NH_3]Mn(HCOO)_3$) is magnetically ordered and exhibits strong coupling between the structure, magnetic ordering, spin splitting, and spin textures. These findings enrich our

https://doi.org/10.1021/jacs.3c14744
J. Am. Chem. Soc. 2024, 146, 13105−13112

fundamental understanding of property manipulation and materials functionality and are likely to stimulate further research. From a practical viewpoint, both structure and magnetic ordering can be manipulated by external fields, which offers promising novel applications in spintronics.

■ ASSOCIATED CONTENT

Supporting Information

The Supporting Information is available free of charge at https://pubs.acs.org/doi/10.1021/jacs.3c14744.

Information on band structure, spin splitting, and spin texture of $[NH_2NH_3]Mn(HCOO)_3$ (PDF)

■ AUTHOR INFORMATION

Corresponding Authors

Ravi Kashikar − *Department of Physics, University of South Florida, Tampa, Florida 33620, United States;* orcid.org/0000-0002-5078-3766; Email: ravik@usf.edu

Inna Ponomareva − *Department of Physics, University of South Florida, Tampa, Florida 33620, United States;* orcid.org/0000-0001-8937-4401; Email: iponomar@usf.edu

Authors

Derick DeTellem − *Department of Physics, University of South Florida, Tampa, Florida 33620, United States*

Partha Sarathi Ghosh − *Glass & Advanced Materials Division, Bhabha Atomic Research Centre, Mumbai 400 085, India;* orcid.org/0000-0001-6803-1725

Yixuan Xu − *Department of Chemistry, University of North Texas, Denton, Texas 76201, United States*

Shengqian Ma − *Department of Chemistry, University of North Texas, Denton, Texas 76201, United States;* orcid.org/0000-0002-1897-7069

Sarath Witanachchi − *Department of Physics, University of South Florida, Tampa, Florida 33620, United States*

Manh-Huong Phan − *Department of Physics, University of South Florida, Tampa, Florida 33620, United States;* orcid.org/0000-0002-6270-8990

Sergey Lisenkov − *Department of Physics, University of South Florida, Tampa, Florida 33620, United States*

Complete contact information is available at: https://pubs.acs.org/10.1021/jacs.3c14744

Notes

The authors declare no competing financial interest.

■ ACKNOWLEDGMENTS

This work was supported by the National Science Foundation under grant no. EPMD-2029800.

■ REFERENCES

(1) Baltz, V.; Manchon, A.; Tsoi, M.; Moriyama, T.; Ono, T.; Tserkovnyak, Y. Antiferromagnetic spintronics. *Rev. Mod. Phys.* **2018**, *90*, 015005.

(2) Jungwirth, T.; Marti, X.; Wadley, P.; Wunderlich, J. Antiferromagnetic spintronics. *Nat. Nanotechnol.* **2016**, *11*, 231−241.

(3) Dresselhaus, G. Spin-orbit coupling effects in zinc blende structures. *Phys. Rev.* **1955**, *100* (2), 580−586.

(4) Even, J.; Pedesseau, L.; Jancu, J.-M.; Katan, C. Importance of spin−orbit coupling in hybrid organic/inorganic perovskites for photovoltaic applications. *J. Phys. Chem. Lett.* **2013**, *4* (17), 2999−3005.

(5) Rashba, E. Properties of semiconductors with an extremum loop. I. cyclotron and combinational resonance in a magnetic field perpendicular to the plane of the loop. *Sov. Phys.-Solid State* **1960**, *2*, 1109.

(6) Soumyanarayanan, A.; Reyren, N.; Fert, A.; Panagopoulos, C. Emergent phenomena induced by spin-orbit coupling at surfaces and interfaces. *Nature* **2016**, *539*, 509−517.

(7) Bihlmayer, G.; Noël, P.; Vyalikh, D. V.; Chulkov, E. V.; Manchon, A. Rashba-like physics in condensed matter. *Nat. Rev. Phys.* **2022**, *4*, 642−659.

(8) Schliemann, J. Colloquium: Persistent spin textures in semiconductor nanostructures. *Rev. Mod. Phys.* **2017**, *89* (1), 011001.

(9) Tao, L.; Tsymbal, E. Y. Persistent spin texture enforced by symmetry. *Nat. Commun.* **2018**, *9* (1), 2763.

(10) Tao, L.; Tsymbal, E. Y. Perspectives of spin-textured ferroelectrics. *J. Phys. D: Appl. Phys.* **2021**, *54* (11), 113001.

(11) Lines, M. E.; Glass, A. M. *Principles and Applications of Ferroelectrics and Related Materials*; Oxford University Press, 2001 02.

(12) Yuan, L.-D.; Wang, Z.; Luo, J.-W.; Rashba, E. I.; Zunger, A. Giant momentum-dependent spin splitting in centrosymmetric low-*z* antiferromagnets. *Phys. Rev. B* **2020**, *102*, 014422.

(13) Egorov, S. A.; Litvin, D. B.; Evarestov, R. A. Antiferromagnetism-induced spin splitting in systems described by magnetic layer groups. *J. Phys. Chem. C* **2021**, *125* (29), 16147−16154.

(14) Yuan, L.-D.; Wang, Z.; Luo, J.-W.; Zunger, A. Strong influence of nonmagnetic ligands on the momentum-dependent spin splitting in antiferromagnets. *Phys. Rev. B* **2021**, *103*, 224410.

(15) Yuan, L.-D.; Wang, Z.; Luo, J.-W.; Zunger, A. Prediction of low-z collinear and noncollinear antiferromagnetic compounds having momentum-dependent spin splitting even without spin-orbit coupling. *Phys. Rev. Mater.* **2021**, *5*, 014409.

(16) Yuan, L.-D.; Zhang, X.; Mera, C.; Zunger, A. Uncovering hidden spin polarization of energy bands in antiferromagnets. *arXiv* **2022**, arXiv:2211.09921.

(17) Hayami, S.; Yanagi, Y.; Kusunose, H. Momentum-dependent spin splitting by collinear antiferromagnetic ordering. *J. Phys. Soc. Jpn.* **2019**, *88* (12), 123702.

(18) Hayami, S.; Yanagi, Y.; Kusunose, H. Bottom-up design of spin-split and reshaped electronic band structures in antiferromagnets without spin-orbit coupling: Procedure on the basis of augmented multipoles. *Phys. Rev. B* **2020**, *102*, 144441.

(19) Zhao, H. J.; Liu, X.; Wang, Y.; Yang, Y.; Bellaiche, L.; Ma, Y. Zeeman effect in centrosymmetric antiferromagnetic semiconductors controlled by an electric field. *Phys. Rev. Lett.* **2022**, *129*, 187602.

(20) Šmejkal, L.; Sinova, J.; Jungwirth, T. Beyond conventional ferromagnetism and antiferromagnetism: A phase with nonrelativistic spin and crystal rotation symmetry. *Phys. Rev. X* **2022**, *12*, 031042.

(21) Šmejkal, L.; Sinova, J.; Jungwirth, T. Emerging research landscape of altermagnetism. *Phys. Rev. X* **2022**, *12*, 040501.

(22) Krempaský, J.; Šmejkal, L.; D'Souza, S. W.; Hajlaoui, M.; Springholz, G.; Uhlířová, K.; Alarab, F.; Constantinou, P. C.; Strocov, V.; Usanov, D.; Pudelko, W. R.; González-Hernández, R.; Birk Hellenes, A.; Jansa, Z.; Reichlová, H.; Šobáň, Z.; Gonzalez Betancourt, R. D.; Wadley, P.; Sinova, J.; Kriegner, D.; Minár, J.; Dil, J. H.; Jungwirth, T. Altermagnetic lifting of kramers spin degeneracy. *Nature* **2024**, *626*, 517−522.

(23) Li, W.; Stroppa, A.; Wang, Z.-M.; Gao, S. *Hybrid Organic-Inorganic Perovskites*; Wiley, 2020.

(24) Popoola, A.; Ghosh, P. S.; Kingsland, M.; Kashikar, R.; DeTellem, D.; Xu, Y.; Ma, S.; Witanachchi, S.; Lisenkov, S.; Ponomareva, I. First-principles property assessment of hybrid formate perovskites. *J. Chem. Phys.* **2023**, *159*, 074702.

(25) Ma, Y.; Sun, Y. Multiferroic and thermal expansion properties of metal-organic frameworks. *J. Appl. Phys.* **2020**, *127*, 080901.

(26) Chen, S.; Shang, R.; Hu, K.-L.; Wang, Z.-M.; Gao, S. $[NH_2NH_3]$ $[M(HCOO)_3]$ (M = Mn^{2+} Zn^{2+} Co^{2+} and Mg^{2+}): structural phase transitions, prominent dielectric anomalies and negative thermal expansion, and magnetic ordering. *Inorg. Chem. Front.* **2014**, *1*, 83−98.

(27) Maczka, M.; Gagor, A.; Ptak, M.; Paraguassu, W.; da Silva, T. A.; Sieradzki, A.; Pikul, A. Phase transitions and coexistence of magnetic and electric orders in the methylhydrazinium metal formate frameworks. *Chem. Mater.* **2017**, *29* (5), 2264−2275.
(28) Ghosh, P. S.; DeTellem, D.; Ren, J.; Witanachchi, S.; Ma, S.; Lisenkov, S.; Ponomareva, I. Unusual properties of hydrogen-bonded ferroelectrics: The case of cobalt formate. *Phys. Rev. Lett.* **2022**, *128*, 077601.
(29) Gunatilleke, W. D. C. B.; Wei, K.; Niu, Z.; Wojtas, L.; Nolas, G.; Ma, S. Thermal conductivity of a perovskite-type metal−organic framework crystal. *Dalton Trans.* **2017**, *46*, 13342−13344.
(30) Lou, F.; Gu, T.; Ji, J.; Feng, J.; Xiang, H.; Stroppa, A. Tunable spin textures in polar antiferromagnetic hybrid organic−inorganic perovskites by electric and magnetic fields. *npj Comput. Mater.* **2020**, *6*, 114.
(31) Yananose, K.; Clark, E. R.; Saines, P. J.; Barone, P.; Stroppa, A.; Yu, J. Synthesis and magnetic properties of the multiferroic $[C(NH_2)_3]Cr(HCOO)_3$ metal-organic framework: The role of spin-orbit coupling and Jahn-Teller distortions. *Inorg. Chem.* **2023**, *62* (42), 17299−17309.
(32) Kashikar, R.; Ghosh, P. S.; Lisenkov, S.; Nanda, B. R. K.; Ponomareva, I. Chemically and electrically tunable spin polarization in ferroelectric cd-based hybrid organic-inorganic perovskites. *Phys. Rev. B* **2021**, *104*, 235132.
(33) Kashikar, R.; Ghosh, P. S.; Lisenkov, S.; Stroppa, A.; Ponomareva, I. Rashba effects in lead-free ferroelectric semiconductor $[CH_3PH_3]SnBr_3$. *Phys. Rev. Mater.* **2022**, *6*, 104603.
(34) Kresse, G.; Furthmüller, J. Efficient iterative schemes for ab initio total-energy calculations using a plane-wave basis set. *Phys. Rev. B* **1996**, *54*, 11169−11186.
(35) Blöchl, P. E. Projector augmented-wave method. *Phys. Rev. B* **1994**, *50*, 17953−17979.
(36) Perdew, J. P.; Burke, K.; Ernzerhof, M. Generalized gradient approximation made simple. *Phys. Rev. Lett.* **1996**, *77*, 3865−3868.
(37) Dudarev, S. L.; Botton, G. A.; Savrasov, S. Y.; Humphreys, C. J.; Sutton, A. P. Electron-energy-loss spectra and the structural stability of nickel oxide: An lsda+u study. *Phys. Rev. B* **1998**, *57*, 1505−1509.
(38) Grimme, S.; Antony, J.; Ehrlich, S.; Krieg, H. A consistent and accurate ab initio parametrization of density functional dispersion correction (DFT-D) for the 94 elements H-Pu. *J. Chem. Phys.* **2010**, *132*, 154104.
(39) King-Smith, R. D.; Vanderbilt, D. Theory of polarization of crystalline solids. *Phys. Rev. B* **1993**, *47*, 1651−1654.
(40) Wang, Z.-C.; Thanabalasingam, K.; Scheifers, J. P.; Streeter, A.; McCandless, G. T.; Gaudet, J.; Brown, C. M.; Segre, C. U.; Chan, J. Y.; Tafti, F. Antiferromagnetic Order and Spin-Canting Transition in the Corrugated Square Net Compound $Cu_3(TeO_4)(SO_4)\cdot H_2O$. *Inorg. Chem.* **2021**, *60* (14), 10565−10571.
(41) Kuo, Y.-L.; Liu, H.-K.; Yang, C.-I. Spin canting and weak ferromagnetism in a new 2D coordination polymer with the CO(II) chain bridged by a single end-to-end azide. *Inorganics* **2023**, *11* (11), 444.
(42) Cao, C.; Liu, S.-J.; Yao, S.-L.; Zheng, T.-F.; Chen, Y.-Q.; Chen, J.-L.; Wen, H.-R. Spin-canted antiferromagnetic ordering in transition metal−organic frameworks based on tetranuclear clusters with mixed v- and y-shaped ligands. *Cryst. Growth Des.* **2017**, *17* (9), 4757−4765.
(43) Kingsland, M.; Ghosh, P. S.; Lisenkov, S.; Ponomareva, I. Structural, electrical, and electromechanical properties of inverse hybrid perovskites from first-principles: The case of $(CH_3NH_3)_3OI$. *J. Phys. Chem. C* **2021**, *125* (16), 8794−8802.
(44) Ponomareva, I. Co and Mn Formate Structures. https://github.com/USFmatscilab/Co-Mn-Formate-AFMG, 2024.
(45) Stroppa, A.; Barone, P.; Jain, P.; Perez-Mato, J. M.; Picozzi, S. Hybrid improper ferroelectricity in a multiferroic and magnetoelectric metal-organic framework. *Adv. Mater.* **2013**, *25* (16), 2284−2290.
(46) Stroppa, A.; Jain, P.; Barone, P.; Marsman, M.; Perez-Mato, J. M.; Cheetham, A. K.; Kroto, H. W.; Picozzi, S. Electric control of magnetization and interplay between orbital ordering and ferroelectricity in a multiferroic metal−organic framework. *Angew. Chem., Int. Ed.* **2011**, *50* (26), 5847−5850.
(47) Di Sante, D.; Stroppa, A.; Jain, P.; Picozzi, S. Tuning the ferroelectric polarization in a multiferroic metal−organic framework. *J. Am. Chem. Soc.* **2013**, *135* (48), 18126−18130.

https://doi.org/10.1021/jacs.3c14744
J. Am. Chem. Soc. 2024, 146, 13105−13112